

## Self-Calibration from Optical Flow and Its Reliability Evaluation

Kenichi Kanatani\*

Department of Computer Science, Gunma University

**Abstract**

An algorithm is presented for 3-D reconstruction from optical flow observed by an uncalibrated camera. We show that by incorporating a statistical model of image noise, we can not only compute a statistically optimal shape but also evaluate its reliability in quantitative terms. We show real-image experiments and discuss the effect of the “gauge” on the uncertainty description.

**1. Introduction**

3-D reconstruction from optical flow has been studied by many researchers [4, 5, 13], but most have assumed that the camera is calibrated. Recently, the *self-calibration* approach using an uncalibrated camera was formulated by Viéville et al. [16] and Brooks et al. [2]. The self-calibration procedure consists of the following steps:

1. We detect optical flow from an image sequence.
2. We compute the *flow fundamental matrices* from the detected flow.
3. We decompose the computed flow fundamental matrices into the motion parameters.
4. We compute the 3-D shape of the scene.

In this paper, we show that by incorporating a statistical model of image noise, we can not only compute a statistically optimal shape but also evaluate its reliability in quantitative terms. We show real-image experiments and discuss the effect of the *gauge* on the uncertainty description.

**2. Optical Flow Detection**

The conventional method for optical flow detection is based on what is known as the *gradient constraint* [11, 12]. However, the resulting flow does not have sufficient accuracy for 3-D reconstruction. Here, we assume that a limited number of salient feature points are traced by template matching and other means with high accuracy.

**3. Fundamental Matrices**

Let  $\{(x_\alpha, y_\alpha)\}$  and  $\{(x'_\alpha, y'_\alpha)\}$ ,  $\alpha = 1, \dots, N$ , be image coordinates of two sets of points on two different images. We define the “flow” and the “mid-point” of the  $\alpha$ th point as

$$\begin{aligned} \hat{\mathbf{x}}_\alpha &= \begin{pmatrix} (x'_\alpha - x_\alpha)/f_0 \\ (y'_\alpha - y_\alpha)/f_0 \\ 0 \end{pmatrix}, \\ \mathbf{x}_\alpha &= \begin{pmatrix} (x_\alpha + x'_\alpha)/2f_0 \\ (y_\alpha + y'_\alpha)/2f_0 \\ 1 \end{pmatrix}, \end{aligned} \quad (1)$$

where  $f_0$  is an appropriate scale factor (e.g., the image size). If noise does not exist, the following *epipolar equation* is satisfied: [2, 5, 6, 13, 16] (throughout this paper, the inner product of the vectors  $\mathbf{a}$  and  $\mathbf{b}$  is denoted by  $(\mathbf{a}, \mathbf{b})$ ):

$$(\mathbf{x}_\alpha, \mathbf{W}\hat{\mathbf{x}}_\alpha) + (\mathbf{x}_\alpha, \mathbf{C}\mathbf{x}_\alpha) = 0. \quad (2)$$

Here,  $\mathbf{W}$  is an antisymmetric matrix, and  $\mathbf{C}$  is a symmetric matrix. They play the same role as the fundamental matrix for finite motion images, so we call them the *flow fundamental matrices*.

The matrices  $\mathbf{W}$  and  $\mathbf{C}$  are not independent of each other. The following relationship holds [2]:

$$(\mathbf{w}, \mathbf{C}\mathbf{w}) = 0, \quad \mathbf{w} = \begin{pmatrix} W_{32} \\ W_{13} \\ W_{21} \end{pmatrix}. \quad (3)$$

We call this the *decomposability condition*<sup>1</sup>.

From  $\{\hat{\mathbf{x}}_\alpha, \mathbf{x}_\alpha\}$ ,  $\alpha = 1, \dots, N$ , the flow fundamental matrices  $\mathbf{W}$  and  $\mathbf{C}$  are computed by a technique called *renormalization* [6, 9]. The program is implemented in C++ and is publicly available<sup>2</sup>. It outputs the estimates  $\hat{\mathbf{W}}$  and  $\hat{\mathbf{C}}$  of the flow fundamental matrices along with their *standard deviations*  $\hat{\mathbf{W}}^{(+)}$ ,  $\hat{\mathbf{W}}^{(-)}$ ,  $\hat{\mathbf{C}}^{(+)}$ , and  $\hat{\mathbf{C}}^{(-)}$ . If, say,  $\mathbf{W}^{(+)}$  and  $\mathbf{W}^{(-)}$  coincide up to three significant digits, the estimate  $\hat{\mathbf{W}}$  is likely to have accuracy up to approximately three significant digits.

**4. Motion Parameters**

We assume that the camera is freely moving and freely changing its focal length. Other camera parameters such as the principal point, the aspect ratio, and the skew angle, which usually do not change in the course of camera motion, are assumed to be

\*Address: Kiryu, Gunma 376-8515 Japan.  
E-mail: kanatani@cs.gunma-u.ac.jp

<sup>1</sup>This corresponds to the constraint that the fundamental matrix for finite motion should have rank 2.

<sup>2</sup><http://www.ail.cs.gunma-u.ac.jp/~kanatani/e>.

calibrated beforehand. Hence, the unknown parameters are the translation velocity  $\mathbf{v}$ , the rotation velocity  $\boldsymbol{\omega}$ , the focal length  $f$ , and its change rate  $\dot{f}$ .

Brooks et al. [2] showed that these parameters can be computed analytically from  $\mathbf{W} = (W_{ij})$  and  $\mathbf{C} = (C_{ij})$ , but their computation involves rather complicated algebraic manipulations. Here, we present an elegant *group-theoretical procedure* derived by expressing quantities in terms of *irreducible representations* of the group of 2-D rotations  $SO(2)$  [3].

Let  $\mathbf{w} = (w_i)$  be the vector defined in eqs. (3), and do the following computation:

$$A = C_{11} + C_{22}, \quad \bar{B} = (C_{11} - C_{22}) + 2iC_{12}, \quad (4)$$

$$\tilde{C} = 2(C_{13} + iC_{23}), \quad D = C_{33}, \quad (5)$$

$$\tilde{w} = w_1 + iw_2, \quad \tilde{w}' = \frac{\bar{B}}{\tilde{w}}, \quad (6)$$

$$\omega'_1 = \Re[\tilde{w}'], \quad \omega'_2 = \Im[\tilde{w}'], \quad (7)$$

$$\omega_3 = -\frac{A + (\tilde{w}, \tilde{w}')}{2w_3}, \quad (8)$$

$$f' = \sqrt{-\frac{D}{(\tilde{w}, \tilde{w}')}}, \quad \tilde{\phi} = \frac{\tilde{C} - f'^2 w_3 \tilde{w}'}{\tilde{w}}, \quad (9)$$

$$\omega_3 = \Re[\tilde{\phi}], \quad \dot{f}' = -f' \Im[\tilde{\phi}], \quad (10)$$

$$\omega_1 = f' \omega'_1, \quad \omega_2 = f' \omega'_2, \quad (11)$$

$$f = f' f_0, \quad \dot{f} = \dot{f}' f_0. \quad (12)$$

$$\mathbf{v} = N \left[ \begin{pmatrix} w_1 \\ w_2 \\ (f/f_0)w_3 \end{pmatrix} \right]. \quad (13)$$

Here,  $i$  is the imaginary unit. The quantities with tildes are complex numbers:  $\Re[\cdot]$  and  $\Im[\cdot]$  denote the real and imaginary parts, respectively. We define the "inner product" of complex numbers  $z = x + iy$  and  $z' = x' + iy'$  by  $(z, z') = xx' + yy'$ . The operation  $N[\cdot]$  designates normalization into a unit vector:  $N[\mathbf{a}] = \mathbf{a}/\|\mathbf{a}\|$ .

In the above procedure,  $\omega_3$  is computed by eq. (8) and by the first of eqs. (10) in two ways. The decomposability condition (3) requires that the two values coincide.

However, a degenerate configuration in which the above computation fails occurs when the camera optical axis moves within the plane spanned by it and the translation velocity  $\mathbf{v}$ , e.g., when the camera undergoes a pure translation or the camera optical axis passes through a fixed point in the scene.

## 5. Correction of Flow

Let  $V_0[\mathbf{x}]$  and  $V_0[\dot{\mathbf{x}}]$  be the covariance matrices of the position  $\mathbf{x}$  and the flow  $\dot{\mathbf{x}}$  defined up to scale. They can be determined from the Hessian of the residual surface of template matching of gray levels [14, 15]. If no prior information is available, we may use the default values  $V_0[\dot{\mathbf{x}}] = 2\text{diag}(1, 1, 0)$  and

$V_0[\mathbf{x}] = \text{diag}(1, 1, 0)/2$ , where  $\text{diag}(\dots)$  denotes the diagonal matrix with diagonal elements  $\dots$  in that order.

In the presence of noise, the data  $\dot{\mathbf{x}}$  and  $\mathbf{x}$  may not necessarily satisfy eq. (2) for the computed flow fundamental matrices  $\mathbf{C}$  and  $\mathbf{W}$ . So, we optimally correct  $\dot{\mathbf{x}}$  and  $\mathbf{x}$  to enforce eq. (2). This is done as follows [6]:

$$\begin{aligned} \hat{\dot{\mathbf{x}}} &= \dot{\mathbf{x}} + \frac{E(\dot{\mathbf{x}}, \mathbf{x})}{V(\dot{\mathbf{x}}, \mathbf{x})} V_0[\dot{\mathbf{x}}] \mathbf{W} \mathbf{x}, \\ \hat{\mathbf{x}} &= \mathbf{x} - \frac{E(\dot{\mathbf{x}}, \mathbf{x})}{V(\dot{\mathbf{x}}, \mathbf{x})} V_0[\mathbf{x}] (\mathbf{W} \dot{\mathbf{x}} + 2\mathbf{C} \mathbf{x}). \end{aligned} \quad (14)$$

Here, we define

$$\begin{aligned} E(\dot{\mathbf{x}}, \mathbf{x}) &= (\mathbf{x}, \mathbf{W} \dot{\mathbf{x}}) + (\mathbf{x}, \mathbf{C} \mathbf{x}), \\ V(\dot{\mathbf{x}}, \mathbf{x}) &= (\mathbf{W} \mathbf{x}, V_0[\dot{\mathbf{x}}] \mathbf{W} \mathbf{x}) \\ &\quad + (\mathbf{W} \dot{\mathbf{x}} + 2\mathbf{C} \mathbf{x}, V_0[\mathbf{x}] (\mathbf{W} \dot{\mathbf{x}} + 2\mathbf{C} \mathbf{x})). \end{aligned} \quad (15)$$

The covariance matrices of the resulting values  $\hat{\dot{\mathbf{x}}}$  and  $\hat{\mathbf{x}}$  are given as follows [6]:

$$\begin{aligned} V_0[\hat{\dot{\mathbf{x}}}] &= V_0[\dot{\mathbf{x}}] - \frac{(V_0[\dot{\mathbf{x}}] \mathbf{W} \mathbf{x})(V_0[\dot{\mathbf{x}}] \mathbf{W} \mathbf{x})^\top}{V(\dot{\mathbf{x}}, \mathbf{x})}, \\ V_0[\hat{\mathbf{x}}] &= V_0[\mathbf{x}] \\ &\quad - \frac{V_0[\mathbf{x}] (\mathbf{W} \dot{\mathbf{x}} + 2\mathbf{C} \mathbf{x})(V_0[\mathbf{x}] (\mathbf{W} \dot{\mathbf{x}} + 2\mathbf{C} \mathbf{x}))^\top}{V(\dot{\mathbf{x}}, \mathbf{x})}. \end{aligned} \quad (16)$$

We assume that errors in  $\dot{\mathbf{x}}$  and  $\mathbf{x}$  are statistically independent, but the corrected values  $\hat{\dot{\mathbf{x}}}$  and  $\hat{\mathbf{x}}$  have the following correlation: [6]:

$$V_0[\hat{\dot{\mathbf{x}}}, \hat{\mathbf{x}}] = \frac{V_0[\mathbf{x}] (\mathbf{W} \dot{\mathbf{x}} + 2\mathbf{C} \mathbf{x})(V_0[\dot{\mathbf{x}}] \mathbf{W} \mathbf{x})^\top}{V(\dot{\mathbf{x}}, \mathbf{x})}. \quad (17)$$

## 6. Focal Length Adjustment

After the focal length  $f$  and its change rate  $\dot{f}$  have been computed, we transform  $\dot{\mathbf{x}}$  and  $\mathbf{x}$  and their covariance matrices as follows (we define  $\mathbf{P}_k = \text{diag}(1, 1, 0)$ ):

$$\begin{aligned} \hat{\dot{\mathbf{x}}} &\leftarrow \frac{f_0}{f} \left( \hat{\dot{\mathbf{x}}} - \frac{\dot{f}}{f} \mathbf{P}_k \mathbf{x} \right), \quad \hat{\mathbf{x}} \leftarrow \text{diag} \left( \frac{f_0}{f}, \frac{f_0}{f}, 1 \right) \hat{\mathbf{x}}, \\ V_0[\hat{\dot{\mathbf{x}}}] &\leftarrow \frac{f_0^2}{f^2} \left( V_0[\dot{\mathbf{x}}] - \frac{2\dot{f}}{f} S[V_0[\hat{\dot{\mathbf{x}}}, \hat{\mathbf{x}}]] + \frac{\dot{f}^2}{f^2} V_0[\hat{\mathbf{x}}] \right), \\ V_0[\hat{\dot{\mathbf{x}}}, \hat{\mathbf{x}}] &\leftarrow \frac{f_0^2}{f^2} \left( V_0[\dot{\mathbf{x}}, \mathbf{x}] - \frac{\dot{f}}{f} V_0[\hat{\mathbf{x}}] \right), \\ V_0[\hat{\mathbf{x}}] &\leftarrow \frac{f_0^2}{f^2} V_0[\mathbf{x}]. \end{aligned} \quad (18)$$

Then, we can view the imaging geometry as if using a perspective camera with unit focal length.

## 7. Depth Computation

The depth  $Z$  of the point  $\mathbf{x}$  is given as follows [6]:

$$Z = -\frac{(\mathbf{v}, \mathbf{S}_x \mathbf{v})}{(\mathbf{v}, \mathbf{S}_x (\hat{\mathbf{x}} + \boldsymbol{\omega} \times \mathbf{x}))}. \quad (19)$$

Here, we define

$$\mathbf{S}_x = \mathbf{Q}_x^\top \mathbf{Q}_x, \quad \mathbf{Q}_x = \mathbf{I} - \mathbf{x} \mathbf{k}^\top, \quad (20)$$

and  $\mathbf{k} = (0, 0, 1)^\top$ . The 3-D position of this point is given by

$$\mathbf{r} = Z \mathbf{x}. \quad (21)$$

At this point, we need to check the sign of the depth. This is because the signs of  $\mathbf{W}$  and  $\mathbf{C}$  are indeterminate as implied by eq. (2). Let  $\hat{Z}_\alpha$  be the depth associated with  $\hat{\mathbf{x}}_\alpha$ . We replace the sign of each  $\hat{Z}_\alpha$  if  $\sum_{\alpha=1}^N \text{sgn}[\hat{Z}_\alpha] < 0$ , where  $\text{sgn}[\cdot]$  is the signature function that takes 1, 0, and  $-1$  for  $x > 0$ ,  $x = 0$ , and  $x < 0$ , respectively.

## 8. Reliability Evaluation

From eq. (21), the covariance matrix of the reconstructed position  $\hat{\mathbf{r}}$  is given up to scale as follows:

$$V_0[\hat{\mathbf{r}}] = \hat{Z}^2 V_0[\hat{\mathbf{x}}] + 2\hat{Z} S[V_0[\hat{Z}, \hat{\mathbf{x}}] \hat{\mathbf{x}}^\top] + V_0[\hat{Z}] \hat{\mathbf{x}} \hat{\mathbf{x}}^\top. \quad (22)$$

The matrix  $V_0[\hat{\mathbf{x}}]$  is given in eqs. (18). From eqs. (19), the matrices  $V_0[\hat{Z}]$  and  $V_0[\hat{Z}, \hat{\mathbf{x}}]$  are given as follows:

$$\begin{aligned} V_0[\hat{Z}] &= \frac{\hat{Z}^4}{(\mathbf{v}, \mathbf{S}_x \mathbf{v})} \text{tr} \left( V_0[\hat{\mathbf{x}}] + 2S[\mathbf{Q}_x (\boldsymbol{\omega} \times V_0[\hat{\mathbf{x}}, \hat{\mathbf{x}}]) \right. \\ &\quad \left. - a V_0[\hat{\mathbf{x}}, \hat{\mathbf{x}}] + \mathbf{Q}_x (\boldsymbol{\omega} \times V_0[\hat{\mathbf{x}}] \times \boldsymbol{\omega}) \mathbf{Q}_x^\top \right. \\ &\quad \left. - 2a S[\mathbf{Q}_x (\boldsymbol{\omega} \times V_0[\hat{\mathbf{x}}])] + a^2 V_0[\hat{\mathbf{x}}] \right), \\ V_0[\hat{Z}, \hat{\mathbf{x}}] &= \frac{\hat{Z}^2}{(\mathbf{v}, \mathbf{S}_x \mathbf{v})} \left( V_0[\hat{\mathbf{x}}, \hat{\mathbf{x}}] \mathbf{Q}_x \mathbf{v} \right. \\ &\quad \left. - V_0[\hat{\mathbf{x}}] (\boldsymbol{\omega} \times \mathbf{S}_x \mathbf{v} + a \mathbf{Q}_x \mathbf{v}) \right). \end{aligned} \quad (23)$$

Here,  $\text{tr}$  denotes trace, and we define

$$a = \frac{(\mathbf{k}, \mathbf{v})}{\hat{Z}} + |\mathbf{k}, \boldsymbol{\omega}, \hat{\mathbf{x}}|. \quad (24)$$

However, this analysis is based on the computed flow fundamental matrices  $\hat{\mathbf{C}}$  and  $\hat{\mathbf{W}}$ . They are computed from the data  $\{\hat{\mathbf{x}}_\alpha, \mathbf{x}_\alpha\}$ ,  $\alpha = 1, \dots, N$ , and hence are not exact. It follows that the values  $f$ ,  $\hat{f}$ ,  $\mathbf{v}$  and  $\boldsymbol{\omega}$  are not exact. However, it is difficult to analyze the error propagation precisely. Here, we adopt the following approximation. We reconstruct two 3-D positions  $\mathbf{r}^{(\pm)}$  for  $\mathbf{x}$  from the standard deviations  $\mathbf{C}^{(\pm)}$  and  $\mathbf{W}^{(\pm)}$  and regard  $(\mathbf{r}^{(+)} - \hat{\mathbf{r}})(\mathbf{r}^{(+)} - \hat{\mathbf{r}})^\top$  as the covariance matrix of  $\mathbf{r}$  due to the errors in  $\hat{\mathbf{C}}$  and  $\hat{\mathbf{W}}$ . The total covariance matrix of  $\hat{\mathbf{r}}$  is given by

$$V[\hat{\mathbf{r}}] = \hat{\epsilon}^2 V_0[\hat{\mathbf{r}}] + (\mathbf{r}^{(+)} - \hat{\mathbf{r}})(\mathbf{r}^{(+)} - \hat{\mathbf{r}})^\top, \quad (25)$$



Figure 1: Real images of an indoor scene.

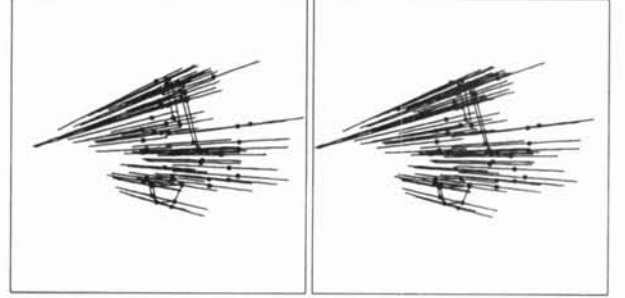


Figure 2: 3-D reconstruction and uncertainty ellipsoids (stereogram).

where  $\hat{\epsilon}^2$  is the absolute noise magnitude, which can be estimated in the process of computing  $\hat{\mathbf{C}}$  and  $\hat{\mathbf{W}}$  [6, 9].

## 9. Real Image Experiment

We reconstructed the 3-D shape from the two images shown in Fig. 1, using the feature points marked in the images. Fig. 2 is a side view of the reconstructed points (stereogram); wireframes are shown for some points. On each reconstructed point is centered the uncertainty ellipsoid defined by the covariance matrix given by eq. (25). All ellipsoids look like thin needles, indicating that the uncertainty is large along the depth orientation.

*This description is deceptive, however.* This uncertainty description is based on a particular *gauge*, i.e., a choice of normalization: the world coordinate system is identified with the camera frame and the translation velocity is normalized to unit length [8, 10]. This gauge hides the fact that the uncertainty is mostly due to that of the translation velocity. In fact, what is uncertain is the depth of the object *as a whole*, not the object shape.

For example, if we take the centroid of the polyhedral object as the coordinate origin and normalize the root-mean-square distance to the vertices from the centroid to unit length, we obtain the description shown in Fig. 3(a). By construction, the uncertainty is almost symmetric with respect to the centroid, and the object shape has very little uncertainty.

Fig. 3(b) is the uncertainty description for yet another gauge: one of the object vertex is taken to be the coordinate origin, another is taken to be  $(1, 1, 0)$ , and a third one is on the  $XY$  plane. By definition, the first two points have no uncertainty.

It follows that *uncertainty of individual quantities has no absolute meaning*. In other words, the discrepancy of the reconstructed quantities from their

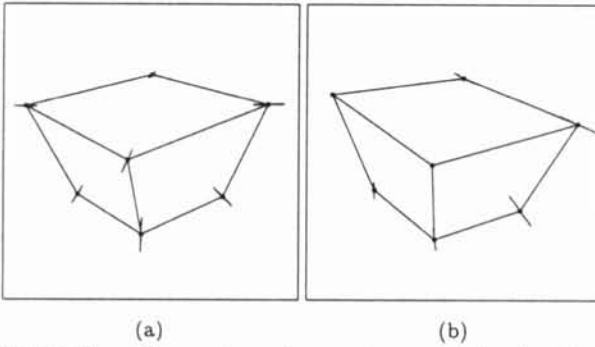


Figure 3: Gauge dependence of uncertainty description. (a) Normalization based on the centroid. (b) Normalization based on three vertices.

	ratio	angle (deg)
computed value	1.02	95.1
true value	1.00	90.0
predicted standard deviation	0.08	17.0

Table 1: Reliability of gauge invariants.

true values is not a meaningful measure of accuracy if artificial normalizations are involved.

Let us call the description changes due to choosing different gauges (i.e., normalizations) *gauge transformations*. Absolute meaning can be given only to *gauge invariants* [8], i.e., quantities invariant to gauge transformations. Typical gauge invariants for Euclidean reconstruction are ratios of lengths and angles of lines. Table 1 lists the ratio of two sides of the polyhedral object and the angle they make along with their true values and their standard deviations derived by the covariance matrices of the vertices.

Fig. 4 shows two real images of a car. Fig. 5 shows its 3-D shape computed from the feature points marked in these images. We defined a wire-frame with triangular meshes from the reconstructed points and mapped the texture onto it. A fairly accurate 3-D shape is created even though only two views are used.

## 10. Concluding Remarks

An algorithm has been presented for 3-D reconstruction from optical flow observed by an uncalibrated camera. We have shown that by incorporating a statistical model of image noise, we can not only compute a statistically optimal shape but also evaluate its reliability in quantitative terms, although the accuracy is not as high as that using the fundamental matrix [1, 7]. We have shown real-image experiments and discussed the effect of the gauge on the uncertainty description.

**Acknowledgments:** This work was in part supported by the Ministry of Education, Science, Sports and Culture, Japan under a Grant in Aid for Scientific Research C(2) (No. 11680377). The author thanks Mike Brooks of the University of Adelaide and his colleagues for collaboration in this research. He also thanks Naoya Ohta of Gunma University and Yoshiyuki Shimizu of Sharp Ltd. for their assistance in doing real image experiments.

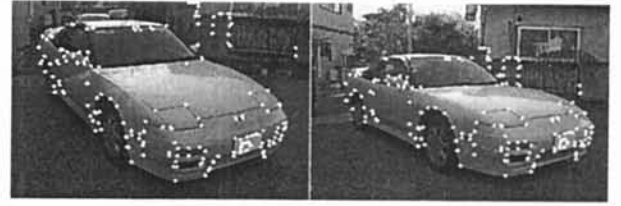


Figure 4: Two images of a car.

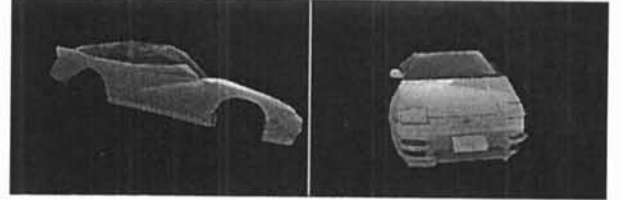


Figure 5: Reconstructed 3-D shape.

## References

- [1] L. Baumela, L. Agapito, P. Bustos and I. Reid, Motion estimation using the differential epipolar equation, *Proc. 15th Int. Conf. Patt. Recogn.*, September 2000, Barcelona, Spain, Vol.3, pp. 848–851.
- [2] M. J. Brooks, W. Chojnacki and L. Baumera, Determining the egomotion of an uncalibrated camera from instantaneous optical flow, *J. Opt. Soc. Am., A*, **14**-10 (1997), 2670-2677.
- [3] K. Kanatani, *Group-Theoretical Methods in Image Understanding*, Springer, Berlin, 1990.
- [4] K. Kanatani, 3-D interpretation of optical flow by renormalization, *Int. J. Comput. Vision*, **11**-3 (1993), 267–282.
- [5] K. Kanatani, *Geometric Computation for Machine Vision*, Oxford University Press, Oxford, 1993.
- [6] K. Kanatani, *Statistical Optimization for Geometric Computation: Theory and Practice*, Elsevier, Amsterdam, 1996.
- [7] K. Kanatani, Gauge-based reliability analysis of 3-D reconstruction from two uncalibrated perspective views, *Proc. 15th Int. Conf. Patt. Recogn.*, September 2000, Barcelona, Spain, Vol.1, pp. 76–79.
- [8] K. Kanatani and D. D. Morris, Gauges and gauge transformations in 3D reconstruction from a sequence of images, *Proc. 4th Asian Conf. Computer Vision*, January 2000, Taipei, Taiwan, pp. 1046 – 1051.
- [9] K. Kanatani, Y. Shimizu, N. Ohta, M. J. Brooks, W. Chojnacki and A. van den Hengel, Fundamental matrix from optical flow: Optimal computation and reliability evaluation, *J. Electronic Imaging*, **9**-2 (2000), 194–202.
- [10] D. D. Morris, K. Kanatani and T. Kanade, Uncertainty modeling for optimal structure from motion, *IEEE Workshop on Vision Algorithms: Theory and Practice*, September 1999, Corfu, Greece, pp. 33–40.
- [11] N. Ohta, Image movement detection with reliability indices, *IEICE Trans.*, **E79**-10 (1991), 3379–3388.
- [12] N. Ohta, Optical flow detection using a general noise model, *IEICE Trans. Inf. & Syst.*, **E79**-D-7 (1996), 951–957.
- [13] N. Ohta and K. Kanatani, Optimal structure-from-motion algorithm for optical flow, *IEICE Trans. Inf. & Sys.*, **E78**-D-12 (1995), 1559–1566.
- [14] J. Shi and C. Tomasi, “Good features to track,” in *Proc. IEEE Conf. Comput. Vision Patt. Recogn.*, June 1994, Seattle, WA, U.S.A., pp. 593–600.
- [15] A. Singh, “An estimation-theoretic framework for image-flow computation,” in *Proc. 3rd Int. Conf. Comput. Vision*, December, 1990, Osaka, Japan, pp. 168–177.
- [16] T. Viéville and O. D. Faugeras, The first order expansion of motion equations in the uncalibrated case, *Comput. Vision Image Understanding*, **64**-1 (1996), 128–146.